Dependence of heat transport and confinement on isotopic composition in conventional H-mode plasmas in JT-60U

H. Urano[1], T. Takizuka[2], M. Kikuchi[1], T. Nakano[1], T. Fujita[1], N. Oyama[1], Y. Kamada[1], N. Hayashi[1] and the JT-60 Team[1]

1) Japan Atomic Energy Agency, Naka Fusion Institute, Naka, Ibaraki 311-0193 Japan

2) Osaka University, Graduate School of Engineering, Suita, Osaka, 565-0871 Japan

e-mail contact of main author: urano.hajime@jaea.go.jp

Dependence of heat transport on isotopic composition is investigated in conventional H-mode plasmas. The identical profiles of n_e, T_e and T_i are obtained for hydrogen and deuterium plasmas while the required power becomes clearly larger for hydrogen, resulting in the reduction of the heat diffusivity for deuterium. The result of the identical temperature profiles in spite of different heating power suggests that the characteristics of heat conduction differs essentially between hydrogen and deuterium even at the same scale length of temperature gradient. The self-regulating physics mechanism determining overall H-mode confinement is also addressed. The edge pedestal pressure is increased by elevated total β_p regardless of the difference of the isotropic composition.

1. Introduction

Knowledge of the influence of the plasma isotopic composition on the heat conduction in the steady H-mode plasma has important consequences from both the physics and the engineering point of view. The effects of the isotope mass M on the energy confinement have been extensively studied [1,2]. For all discharge types the energy confinement increased with isotope mass $\tau_{th} \propto M^{\zeta}$ with the exponent ζ greater than 0. However, little is known about the process responsible for the energy confinement by varying the isotopic composition. In this paper, dependence of hydrogen isotopes on heat transport and pedestal structure is characterized using hydrogen and deuterium H-mode plasmas in JT-60U tokamak.

H-mode plasma is characterized by an edge pedestal component which is determined by the magnetohydrodynamic (MHD) destabilization of edge-localized-modes (ELMs) and a core component which is governed by the turbulent transport that originates in the micro-instabilities. In present understanding particularly of the core plasma, it is believed that turbulence driven by ion temperature gradient (ITG) is the main cause for the anomalous heat transport through the ion channel in tokamaks [3, 4]. The ion temperature profiles are limited by a strong increase in the transport when the temperature gradient scale length $L_{T_i}(= T_i/\nabla T_i)$ exceeds the critical value $L^c_{T_i}$. Under this situation the ion heat diffusivity χ_i can be described by:

$$\chi_i = \chi_{i0} + \xi_{TG} \cdot f\left(R/L_{T_i} - R/L^c_{T_i}\right) \quad (1)$$

where χ_{i0} represents the ion heat diffusivity in the absence of TG turbulence, which consists mainly of neoclassical transport, and R is the major radius. The product $\xi_{TG} \cdot f$ represents the ion heat diffusivity caused by the ITG turbulence. The function f is equal to zero for $L_{T_i} \geq L^c_{T_i}$ but increases rapidly when $L_{T_i} < L^c_{T_i}$. When $L_{T_i} < L^c_{T_i}$ transport is enhanced to keep L_{T_i} close to $L^c_{T_i}$ providing the stiff temperature profile.

Experimental observations of the strong correlation between the edge and core T_i values serve as qualitatively supportive evidence of this theoretical picture [5–8]. For the interest of predicting the energy confinement that would lead to possible fusion power in a reactor, the experimental characterization of heat transport has been well developed. However, little is known about the processes responsible for heat transport by varying the hydrogen isotope composition. The modeling such anomalous transport processes for H-mode plasmas strongly requires the experimental evidence obtained from a set of different isotope species. The study on the isotope effect on the energy confinement was originally motivated by the fact that

the enhancement of the ion heat transport which depends on the ion Larmor radius ρ_i ($\propto M^{1/2}$) in most theoretical models, such as gyro-Bohm diffusion, apparently contradicts the observation of the enhanced confinement obtained with heavy hydrogen isotopes.

This article presents the dependence of heat transport on the hydrogen isotope mass in conventional H-mode plasmas from the view point of the TG scale length of the ion temperature profiles at the plasma core. In addition, the self-regulating physics mechanism determining overall H-mode confinement is also addressed.

2. Heat transport properties

2.1 Experiments on H-mode plasmas

A series of experiments on hydrogen and deuterium H-mode plasmas using variable heating power with a neutral beam (NB) was analyzed in JT-60U tokamak. The experiments were conducted at a plasma current $I_p = 1.08$MA and a toroidal magnetic field $B_t = 2.4$T at a given magnetic geometry with a major radius $R = 3.36$m and a minor radius $a = 0.86$m [9]. The remaining geometrical parameters were also fixed with an ellipticity $\kappa = 1.4$, a triangularity $\delta = 0.36$ and a safety factor at 95 % flux surface $q_{95} = 3.7$. The line-averaged electron density remained nearly constant at $\bar{n}_e = 2.3-2.5\times10^{-19}$m^{-3}. A positive-ion-based NB (PNB) with an accelerating energy E_b of $\sim$ 85keV was applied in the P_{NBI} range of 5−15MW, which was sufficient to examine the ITG scale length relative to the local ion heat flux.

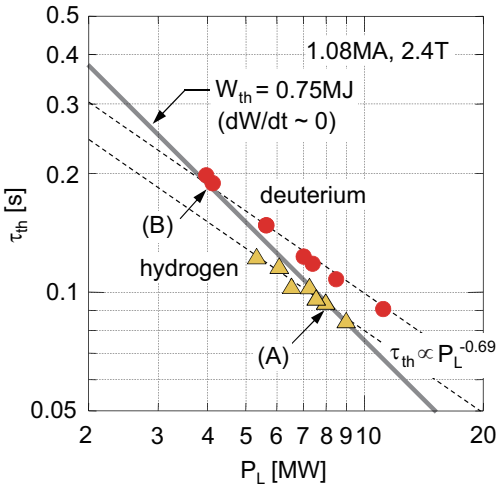

FIG. 1: Dependence of the thermal energy confinement time τ_{th} on the loss power P_L for deuterium and hydrogen H-mode plasmas performed at 1.08MA and 2.4T. A pair of plasmas with $W_{th}(= P_L\tau_{th})$ of 0.75MJ are indicated as (A) and (B).

Fig. 1 shows the thermal energy confinement time τ_{th} as a function of the loss power P_L in this series of experiments. The τ_{th} value decreases continuously with P_L for both hydrogen and deuterium at approximately the same scale, as expected from the empirical law $\tau_{th} \propto P_L^{-0.69}$ [10]. However, τ_{th} is larger by approximately a factor of 1.2−1.3 for deuterium in comparison with that for hydrogen at a given P_L. The effective ion charge number Z_{eff} is $\sim$ 1.5 at $P_L \lesssim$ 5MW in both cases. The Z_{eff} for deuterium increases continuously with the heating power and reaches $\sim$ 2.4 at P_L of $\sim$ 8MW, while it remains constant at $\sim$ 1.5 for hydrogen.

2.2 Heat transport analysis at a given thermal energy

The gray line in Fig. 1 indicates the constant thermal stored energy W_{th} (= 0.75MJ) when a steady state ($dW/dt \sim 0$) is reached. A pair of hydrogen and deuterium plasmas with the same W_{th} were chosen along this line for comparison of the heat transport analysis, as indicated by (A) and (B), respectively. The power required to sustain the same W_{th} was greater for hydrogen ($P_L = 8.0$MW) than for deuterium ($P_L = 4.0$MW) by a factor of two, resulting in the τ_{th} value ($= W_{th}/P_L$) of 0.1s for hydrogen, which was half that for deuterium ($\tau_{th} = 0.2$s). The Z_{eff} value of $\sim$ 1.5 was nearly the same for both cases. The heat diffusivity is estimated by the 1.5-dimensional (two-dimensional equilibrium and one-dimensional transport) transport analysis code (TOPICS) [11].

Figures 2(a)−(f) show the spatial profiles of ion temperature T_i, electron temperature T_e, electron density n_e, toroidal rotation velocity V_T, ion conductive heat flux Q_i and ion

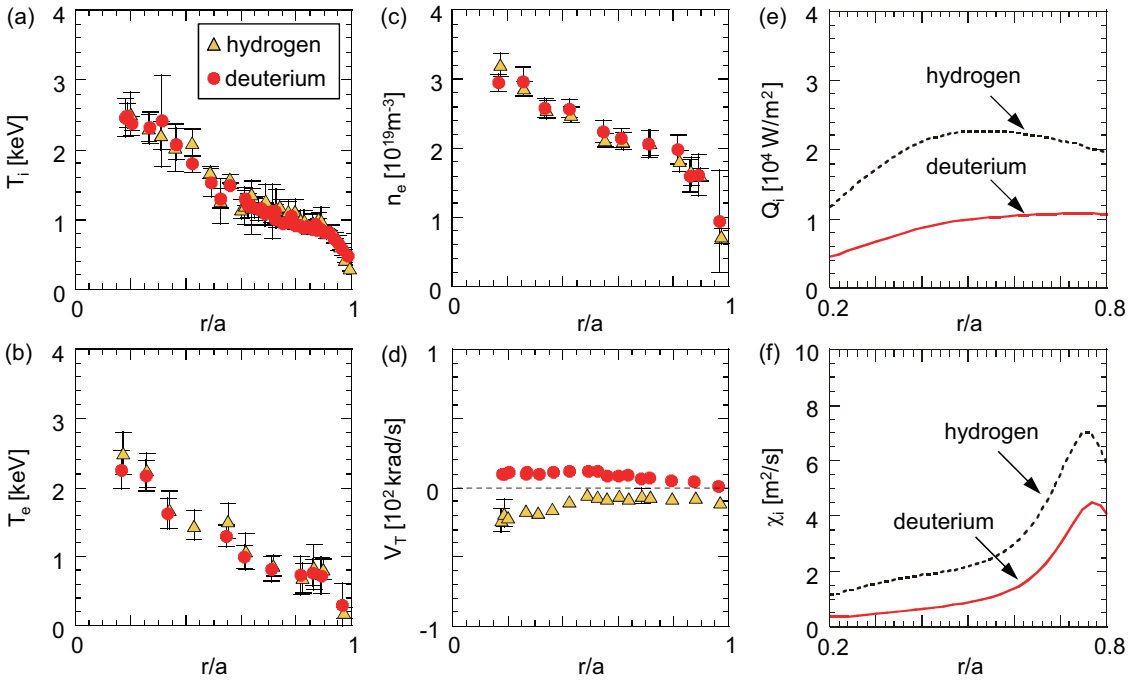

FIG. 2: Profiles of T_i, T_e, n_e, V_T, Q_i, and χ_i which correspond to the hydrogen and deuterium discharges with the same W_th of 0.75MJ.

heat diffusivity χ_i for these two cases, respectively. The spatial profiles of T_i, T_e and n_e become obviously identical across the whole radial range from the edge pedestal shoulder to the center (see Figs. 2(a)−(c)), indicating that the spatial profiles of the thermal pressures p_th, and thus the W_th values, also become approximately identical. The Q_i for hydrogen becomes approximately two times that for deuterium (see Fig. 2(e)), which corresponds to the result that two times as much heating power is required for hydrogen. Hence, the χ_i values for hydrogen are explicitly higher throughout the minor radius compared with those for deuterium as shown in Fig. 2(f). The source heat flux of ions is responsible for nearly 40% of the total source heat flux for both cases. Besides, the Q_i occupies $\sim 70\%$ of the ion source heat flux.

The spatial profile of V_T for hydrogen becomes slightly in more counter than that for deuterium. In this experiment, higher P_NBI is applied for hydrogen using the perpendicular NB to sustain W_th to a similar value. The perpendicular NB enhances the losses of fast ions which drive the toroidal rotation V_T in the counter-direction [12, 13]. This counter-shift might be explained by the NTV driven torque that depends on ∇T_i in the edge steep gradient region and the $j \times B$ torque due to the ripple loss of fast ions [14, 15]. Besides, due to lower neutralization efficiency of NBI for hydrogen, which becomes half that for deuterium, a larger number of perpendicular NB units were injected even at the same P_L for hydrogen to compensate for a shortage of P_NBI in comparison with the P_NBI range for deuterium. This operation also leads to a larger ripple loss of fast ions. The V_T profiles accompanied by

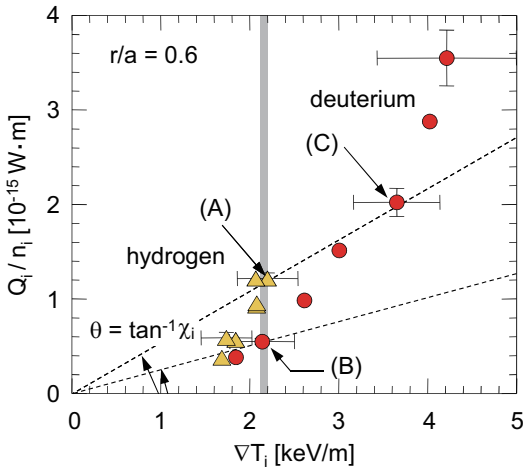

FIG. 3: Relationship between $Q_\mathrm{i}/n_\mathrm{i}$ and ∇T_i evaluated at $r/a = 0.6$. The data for hydrogen and deuterium with the same W_th of 0.75MJ are indicated as (A) and (B), respectively.

low toroidal rotation and low velocity shear indicate that the isotopic differences in energy confinement are apparently not a result of differences in $E \times B$ shear at the plasma core.

Since χ_i in the power balance equation is determined by $Q_i/n_i\nabla T_i$ in the steady state, the ion heat transport can be characterized in a diagram of the ion conductive heat flux divided by the ion density Q_i/n_i and the ion temperature gradient ∇T_i. As shown in Fig. 3, the (Q_i/n_i, ∇T_i) diagram is evaluated at $r/a = 0.6$, where the influence of the local heat transport on the overall energy confinement becomes significant in standard H-mode plasmas. In this diagram, the angle θ formed between the horizontal axis and a straight line that passes through both the data and the origin of the coordinates corresponds to the ion heat diffusivity $\chi_i(= \tan\theta)$. Because the increase in ∇T_i is less significant than that in Q_i/n_i, χ_i increases gradually with the heating power for both hydrogen and deuterium. In further detail, the increase in χ_i with the heating power is more rapid for hydrogen than for deuterium, suggesting a reduced energy confinement for hydrogen plasmas. Simultaneously, the increase in ∇T_i is less intense for hydrogen than for deuterium. In Fig. 3, the data points (A) and (B) with the same W_{th} of 0.75MJ are plotted along the same ∇T_i of $\simeq$ 2.1keV/m at $r/a = 0.6$ because of the identical T_i profiles. However, the Q_i/n_i value increases for hydrogen compared with that for deuterium by a factor of two, resulting in a χ_i value that is two times as large for hydrogen.

2.3 Heat transport analysis at a given heat diffusivity

Along the straight line passing through the hydrogen data point (A), there is a deuterium data point indicated as (C) in Fig. 3. This pair of hydrogen and deuterium plasmas have similar χ_i values of $3.0 - 3.1\mathrm{m}^2/\mathrm{s}$ at $r/a = 0.6$ while both ∇T_i and Q_i/n_i are higher for deuterium (C) than for hydrogen (A). Fig. 4 shows the results of the heat transport analysis for these two cases. The values of T_i and T_e increase for deuterium throughout the minor radius to a greater extent in comparison with those for hydrogen while the n_e profiles are nearly identical (see Figs. 4(a)−(c)). The Z_{eff} of ~ 2.3 for deuterium is higher than the Z_{eff}

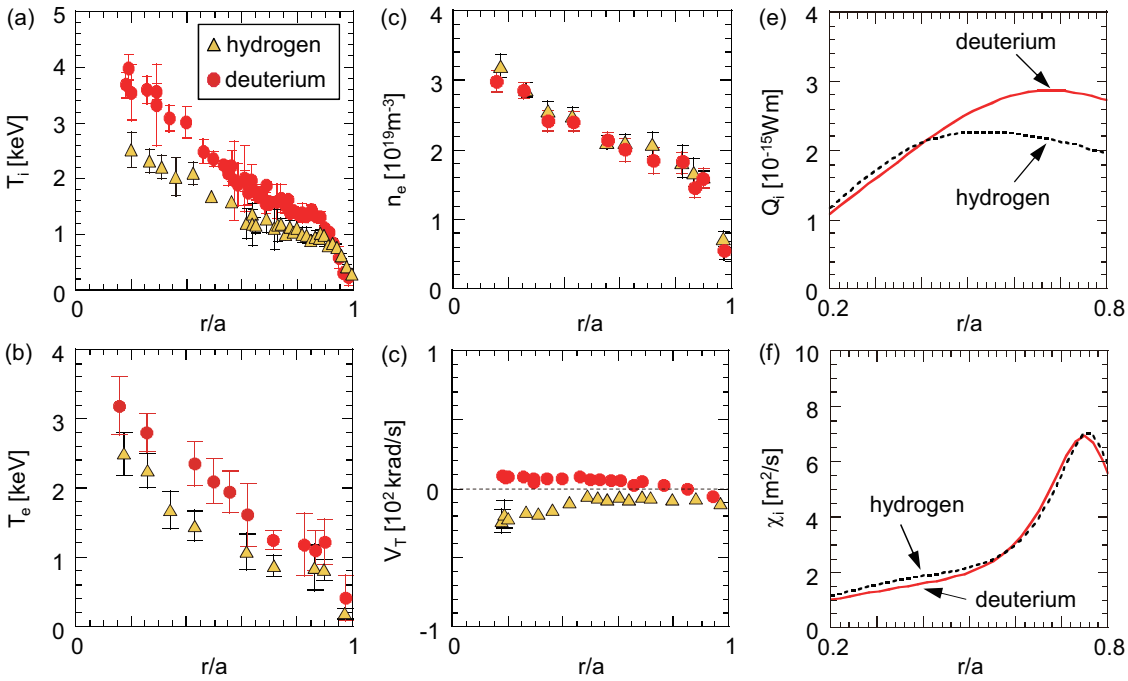

FIG. 4: Profiles of (a) T_i, (b) n_e, (c) Q_i, and (d) χ_i for the hydrogen and deuterium plasmas with similar χ_i values indicated as (A) and (C) in Fig. 3.

of ~ 1.5 for hydrogen, indicating that the deuterium ion density is lower by $\sim 20\%$ than the hydrogen ion density on the assumption that carbon is the main impurity content. The Q_i value for deuterium at $r/a > 0.4$ increases in comparison with that for hydrogen (see Fig. 4(e)), and the spatial profiles of χ_i are nearly identical (see Fig. 4(f)). Despite having nearly the same profiles of Q_i and χ_i at $r/a \leq 0.4$, the higher T_i for deuterium evidently leads to a contribution from the outside of the flux surface as a boundary condition for the profile stiffness. The spatial profile of V_T for hydrogen plasma becomes relatively in more counter than that for deuterium plasma due to the same reason described in section 2.2 (see Fig. 4(d)).

Note that the P_L values for hydrogen (A) and deuterium (C) are 8.0MW and 7.4MW, respectively, while the ion conductive heat flux Q_i of 2.2×10^4W/m^2 at $r/a = 0.6$ is smaller for (A) in comparison with Q_i of 2.7×10^4W/m^2 for (C). This difference in results occurs because the critical energy E_c of the NBI where the power transferred to the ions becomes equivalent to that of the electrons scales as $E_c \propto M^{1/3}$. Under the condition with the accelerating energy E_b of 85keV, which is basically below or comparable to the E_c in standard H-mode plasmas for both hydrogen and deuterium, the fraction of the ion heating power becomes relatively more dominant for deuterium by a factor of $2^{1/3}$ in comparison with that for hydrogen at a given P_L. Accordingly, the resultant Q_i value is higher as shown in Fig. 4(e).

2.4 Scale length of ion temperature gradient

Fig. 5 shows the relationship between χ_i and $\nabla T_i/T_i$ (or R/L_{T_i}) at $r/a = 0.6$. It can be seen in this figure that χ_i increases rapidly with $\nabla T_i/T_i$ for both the hydrogen and deuterium plasmas, indicating the profile stiffness in the ITG unstable region for the variation of the heating power in this experiment. However, the $\nabla T_i/T_i$ values required for a given χ_i clearly increased by a factor of ~ 1.2 for deuterium in comparison with those for hydrogen, as is shown with the plotted pair of data points (A) and (C), which have similar χ_i at different $\nabla T_i/T_i$. On the other hand, this figure also shows the pair of data points (A) and (B) with the same W_{th} of 0.75MJ. As expected from the identical T_i profiles shown in Fig. 2, the Q_i, or χ_i, at $r/a = 0.6$ is two times as large for hydrogen than for deuterium with the same $\nabla T_i/T_i$ of ~ 2.0m^{-1} (or $R/L_{T_i} \sim 7.0$); considering the characteristics of the rapid increase in χ_i with $\nabla T_i/T_i$ (or R/L_{T_i}) for a certain hydrogen isotope species, this result is also indicative of a decrease in the L_{T_i} value with increasing hydrogen isotope mass [17].

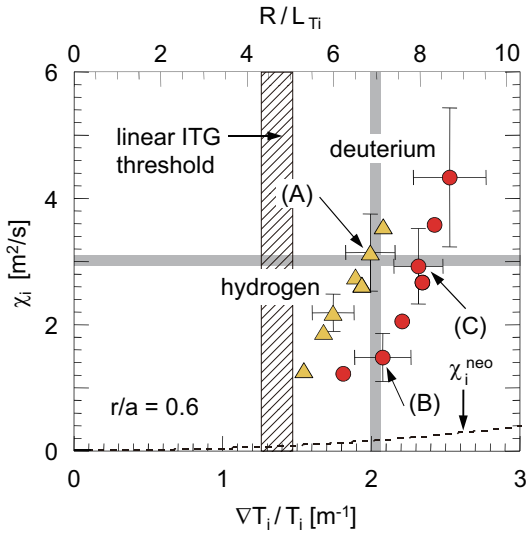

FIG. 5: Relationship between χ_i and $\nabla T_i/T_i$ (or R/L_{T_i}) evaluated at $r/a = 0.6$.

A region of the linear ITG threshold predicted in Refs. [18] and [19] is also indicated in Fig. 5. This threshold value depends on the s/q, T_i/T_e, and ϵ where s and ϵ denote the magnetic shear and the inverse aspect ratio, respectively. The operation with a fixed magnetic geometry enables s/q and ϵ to remain nearly constant. In addition, T_i/T_e also remained at a nearly constant value of $1.1 - 1.3$ at $r/a = 0.6$ for both the hydrogen and deuterium plasmas as Q_i was varied. Accordingly, there is no expected difference in the linear ITG threshold between hydrogen and deuterium. All the experimental data are above the threshold value for the ITG unstable region at $L_{T_i} < L^c_{T_i}$. While the L_{T_i} values in the sufficiently heated phase are clearly smaller for deuterium than those for hydrogen, it is hard

to identify whether the ITG threshold $L_{T_i}^c$ becomes certainly smaller for deuterium in this series of experiments.

3. Self-regulating physics of H-mode plasmas

3.1 Edge pedestal characteristics

The edge pedestal condition plays a significant role in determining the overall confinement in H-mode plasmas. It is therefore important to analyze the energy confinement in hydrogen and deuterium H-mode plasmas by focusing the edge pedestal characteristics.

Fig. 6(a) shows the ELM frequency $f_{\rm ELM}$ as a function of the power crossing the separatrix $P_{\rm sep}$. In this figure, $P_{\rm sep}$ is evaluated by the definition of $P_{\rm L} - P_{\rm rad} - {\rm d}W/{\rm d}t$ where $P_{\rm rad}$ indicates the radiation power from the main plasma. Linear increase of $f_{\rm ELM}$ with $P_{\rm sep}$ for both cases indicates a typical feature of type-I ELMy H-mode plasmas. At a given $P_{\rm sep}$ of $\sim$ 6.5MW (see gray line in Fig. 6(a)), $f_{\rm ELM}$ for hydrogen becomes approximately two times as large for deuterium. The ELM frequency $f_{\rm ELM}$ for the case of hydrogen becomes 165Hz while $f_{\rm ELM}$ for the case of deuterium becomes 80Hz.

Fig. 6(b) shows the relationship between the ELM energy loss $\Delta W_{\rm ELM}$ and the normalized ELM frequency $f_{\rm ELM}/P_{\rm sep}$. The $\Delta W_{\rm ELM}$ becomes smaller roughly by a factor of ~ 2 on the average for hydrogen than that for deuterium. In $(f_{\rm ELM}/P_{\rm sep}, \Delta W_{\rm ELM})$ space, the product of both quantities indicates the fraction of ELM loss in the separatrix power or $P_{\rm ELM}/P_{\rm sep}$. The ELM loss power $P_{\rm ELM}$ $(= f_{\rm ELM}\Delta W_{\rm ELM})$ for deuterium remains $\sim$ 20% of $P_{\rm sep}$ while it is $\sim$ 10% of $P_{\rm sep}$ for hydrogen. The result indicates that the inter-ELM transport power for deuterium is smaller than that for hydrogen. At a given $P_{\rm sep}$, the thermal energy confinement time between ELMs $\tau_{\rm th}^{\rm int}$ for deuterium becomes larger by a factor of ~ 1.4 than that for hydrogen.

Fig. 6(c) shows the edge $T_{\rm i}$ profiles at $P_{\rm L} = 7.3 - 7.4$MW, which corresponds to $P_{\rm sep}$ of $\sim$ 6.5MW indicated in Fig. 6(a). Despite a given $P_{\rm L}$, the $T_{\rm i}$ value at the pedestal shoulder becomes higher for deuterium by a factor of ~ 1.5 than for hydrogen. Note that the total poloidal beta $\beta_{\rm p}^{\rm TOT}$ of 0.9 for deuterium is larger than $\beta_{\rm p}^{\rm TOT}$ of 0.6 for hydrogen.

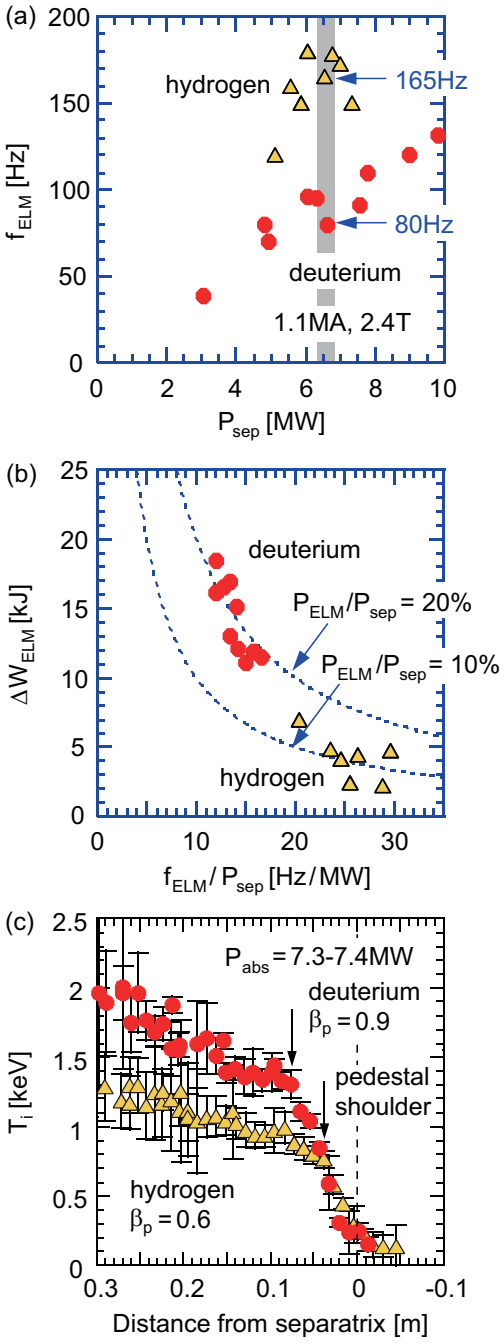

FIG. 6: (a) Dependence of $f_{\rm ELM}$ on $P_{\rm sep}$ for hydrogen and deuterium plasmas. (b) Relation between $\Delta W_{\rm ELM}$ and $f_{\rm ELM}/P_{\rm sep}$. (c) Edge $T_{\rm i}$ profiles at $P_{\rm sep}$ of $7.3 - 7.4$MW.

3.2 Edge stabilization due to high $\beta_{\rm p}$ H-mode plasmas

In the present understanding, H-mode confinement is determined by the relation of two physics processes: (i) the increase of the pedestal temperature as a boundary condition

affecting the reduction in the core heat transport through the profile stiffness, (ii) the increase of total β_p improving the edge stability limit. Fig. 7(a) shows the electron pedestal $n-T$ diagram at a given P_L of $8-9$MW for hydrogen and deuterium H-mode plasmas. The electron pedestal pressure p_e^{ped} evidently differs nearly by a factor of ~ 1.5 between hydrogen and deuterium plasmas at a given P_L. The difference of p_e^{ped} is mainly attributed to the difference of T_e^{ped} while n_e^{ped} remains nearly constant. It is known that the edge stability can be improved by the increase in β_p^{TOT} or Shafranov shift [21–24]. Fig. 7(b) shows the relationship between the total poloidal beta β_p^{TOT} and the pedestal poloidal beta β_p^{ped} for hydrogen and deuterium plasmas. The β_p^{ped} is increased linearly with the increased β_p^{TOT} for both cases. A significant result seen in this figure is that despite the two types of isotope species of hydrogen and deuterium the relationship between β_p^{TOT} and β_p^{ped} is almost identical, which is consistent with the result obtained from the JT-60 confinement database at 1MA and 2T [25]. This result suggests that the increase in β_p^{ped} is strongly affected by the increase in β_p^{TOT} regardless of the difference of the hydrogen isotope species.

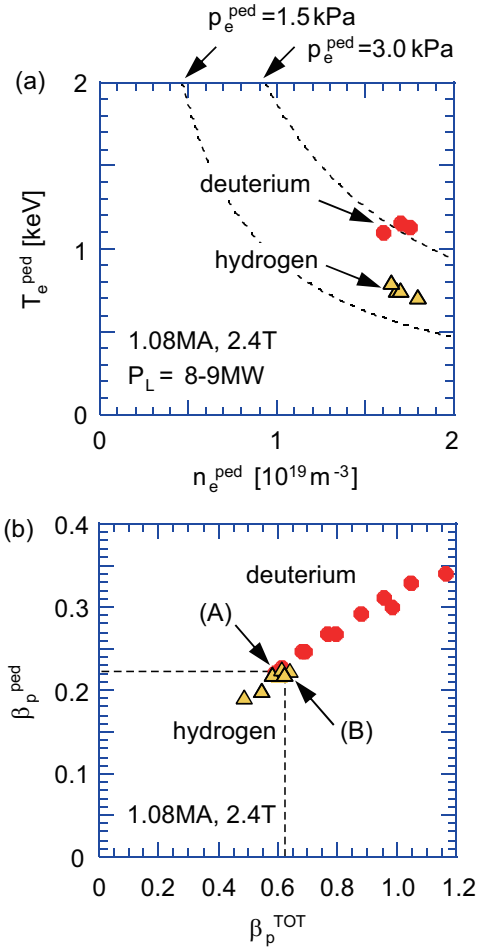

FIG. 7: (a) The relationship between n_e^{ped} and T_e^{ped} at P_L of $8-9$MW for hydrogen and deuterium H-mode plasmas. (b) The relationship between β_p^{TOT} and β_p^{ped}.

In other words, higher pedestal pressure observed for deuterium is obtained by higher β_p^{TOT}. Then, this drives us to the next question how the β_p^{TOT} becomes larger for deuterium than that for hydrogen. A smaller χ_i or L_{T_i} for deuterium is one of the keys leading to higher β_p^{TOT} as the contribution from thermal component. In addition, the fast ion energy depends on the slowing down time of high energy ions τ_s which is proportional to $M^{1/2}T^{3/2}/n$, which also contributes to raise β_p^{TOT} for deuterium. For example, under the condition where the T_i values becomes higher for deuterium by a factor of ~ 1.5 than that for hydrogen at a given P_L, the τ_s or the fast ion component of β_p becomes larger by ~ 2.5 for deuterium. A pair of the data (A) and (B) with the same W_{th} of 0.75MJ (see Fig. 2) are indicated in Fig. 7(b). The fast ion energy of ~ 0.2MJ for the hydrogen (A) is also similar to the deuterium (B) because higher heating power injected in the hydrogen (A) raises the fast ion energy, leading to the same β_p^{TOT}.

When hydrogen isotope mass for a main plasma is changed to be the greater, the reduction in ITG-driven heat transport and the increase in the slowing down time of high energy ions lead to the increase in β_p^{TOT}. This increase of β_p^{TOT} or Shafranov shift improves the edge stability limit and raise the pedestal pressure. The increased pedestal pressure is directly reflected to the increased pedestal temperature while the pedestal density remains nearly constant. Then, the elevated pedestal temperature plays a role as a boundary condition in enhancing the local temperature gradient in the plasma core, resulting in more favorable confinement at heavier hydrogen isotope.

4. Conclusions

Dependence of heat transport on isotopic composition was investigated in conventional H-mode plasmas in this paper. The $\tau_{\rm th}$ value becomes larger by a factor of $\sim 1.2-1.3$ for deuterium than for hydrogen at a given $P_{\rm L}$. When $W_{\rm th}$ was fixed, the profiles of $n_{\rm e}$, $T_{\rm e}$ and $T_{\rm i}$ became identical for both cases while higher heating power was required for hydrogen. The ion conductive heat flux $Q_{\rm i}$ for hydrogen became approximately two times that for deuterium, corresponding to a required heating power to sustain the same $W_{\rm th}$ value that was two times as large for hydrogen. Hence, the $\chi_{\rm i}$ values for hydrogen were higher, explicitly throughout the minor radius, than those for deuterium at the same $L_{\rm T_i}$. The $\nabla T_{\rm i}/T_{\rm i}$, or the inverse of $L_{\rm T_i}$, required for a given $\chi_{\rm i}$ increased by a factor of ~ 1.2 for deuterium compared with that for hydrogen. These results lead to the conclusion that the $L_{\rm T_i}$ is shrunk with hydrogen isotope mass in H-mode plasmas.

The self-regulating physics mechanism determining overall H-mode confinement was also addressed. The relation between $\beta_{\rm p}^{\rm TOT}$ and $\beta_{\rm p}^{\rm ped}$ was almost identical regardless of the difference of the isotope species, suggesting that higher pedestal pressure observed for deuterium H-modes be obtained through higher $\beta_{\rm p}^{\rm TOT}$. In addition to a smaller $\chi_{\rm i}$ or $L_{\rm T_i}$ for deuterium as the contribution from thermal component, the fast ion energy determined by the slowing down time of high energy ions $\tau_{\rm s} \propto M^{1/2}T^{3/2}/n$ is one of the keys leading to higher $\beta_{\rm p}^{\rm TOT}$ for deuterium.

References

[1] Sabbagh, S. A., et al., in Plasma Physics and Nuclear Fusion Research 1994 (Proc. 15th Int. Conf. Seville, 1994) vol. 1, IAEA, Vienna (1994) 663.
[2] Cordey, J. G., et al., Nucl. Fusion **39** (1999) 301.
[3] Kotschenreuter, M., et al., Phys. Plasmas **2** (1995) 2381.
[4] Dimits, A., et al., Phys. Plasmas **7** (2000) 969.
[5] Urano, H., et al., Nucl. Fusion **42** (2002) 76.
[6] Tardini, G., et al., Nucl. Fusion **42** (2002) 258.
[7] Peeters, A. G., et al., Nucl. Fusion **42** (2002) 1376.
[8] Mikkelsen, D. R., et al., Nucl. Fusion **43** (2003) 30.
[9] Urano, H., et al., Nucl. Fusion **48** (2008) 045008.
[10] ITER Physics Basis, Nucl. Fusion **39** (1999) 2175.
[11] Shirai, H., et al., Plasma Phys. Control. Fusion **42** (2000) 1193.
[12] Koide, Y., et al., in Plasma Physics and Nuclear Fusion Research 1992 (Proc. 14th Int. Conf. Würzburg, 1992) vol. 1, IAEA, Vienna (1993) 777.
[13] Urano, H., et al., Nucl. Fusion **47** (2007) 706.
[14] Honda, M., et al., Nucl. Fusion **48** (2008) 085003.
[15] Yoshida, M., et al., Nucl. Fusion **52** (2012) 023024.
[16] Aiba, N., et al., Nucl. Fusion **51** (2011) 073012.
[17] Urano, H., et al., Phys. Rev. Lett. **109** (2012) (in press).
[18] Guo, S. C. and Romanelli, F., Phys. Fluids B **5** (1993) 520.
[19] Jenko, F., et al., Phys. Fluids B **8** (2001) 4096.
[20] Urano, H., et al., Nucl. Fusion **48** (2008) 045008.
[21] Kamada, Y., et al., Plasma Phys. Control. Fusion **48** (2006) A419.
[22] Maggi, C. F., et al., Nucl. Fusion **47** (2007) 535.
[23] Snyder, P. B., et al., Nucl. Fusion **47** (2007) 961.
[24] Leonard, A. W., et al., Phys. Plasmas **15** (2008) 056114.
[25] Urano, H., et al., Nucl. Fusion (in press).